Theoretical analysis of the radius of semiconductor nanowires grown by the catalytic vapour–liquid–solid mechanism

2006 J. Phys.: Condens. Matter 18 3875

(http://iopscience.iop.org/0953-8984/18/15/029)

INSTITUTE OF PHYSICS PUBLISHING JOURNAL OF PHYSICS: CONDENSED MATTER

J. Phys.: Condens. Matter **18** (2006) 3875–3885 doi:10.1088/0953-8984/18/15/029

Theoretical analysis of the radius of semiconductor nanowires grown by the catalytic vapour–liquid–solid mechanism

S Joon Kwon[1] **and Jae-Gwan Park**

Materials Science and Technology Division, Korea Institute of Science and Technology (KIST), PO Box 131, Cheongryang, Seoul 130-650, Korea

E-mail: cheme@kist.re.kr (S J Kwon)

Received 10 October 2005
Published 30 March 2006
Online at stacks.iop.org/JPhysCM/18/3875

Abstract

We present a theoretical analysis of the radius, r_C^*, of semiconductor nanowires (SNWs) grown by the catalytic vapour–liquid–solid (VLS) mechanism. Two types of the catalytic metal were examined, namely case I: thin film, and case II: colloids or cluster. In case I, the number density along with the inter-distance between two neighbouring nucleus, D, and the critical radius of the catalytic metal nucleus, R_C^*, were correlated and determined by either the thermodynamic relationship (determination of R_C^* followed by D) or structural instability (determination of D followed by R_C^*). In case II, the linearly scaling behaviour of r_C^* with the observed radius of the SNWs was explained by comparing with experimental data obtained from the literature. Commonly in both cases, it was shown that r_C^* is thermodynamically determined, assuming the kinetic effect due to the initial diffusion length of the gaseous semiconductor precursor in the early stages of the growth of the SNWs, and that r_C^* mirrors R_C^* only when r_C^* is greater than R_C^*. We also found that the theoretical analysis of r_C^* is matched well with experimental data in the literature.

1. Introduction

One-dimensional (1D) semiconductor nanomaterials can be prepared via a multitude of different routes, for example, the vapour–liquid–solid (VLS) mechanism [1–13], epitaxial growth processes involving self-assembly [14] and organization [15], and spontaneous shape transition [16]. These materials not only offer the possibility of reducing and miniaturizing the feature size of high performance devices and enhancing the quantum confinement effects, but also superior performance for nano- and micro-electronic devices [8, 11]. Since Wagner and Ellis suggested the VLS mechanism to elucidate the growth of large whiskers [17], the

[1] Author to whom any correspondence should be addressed.

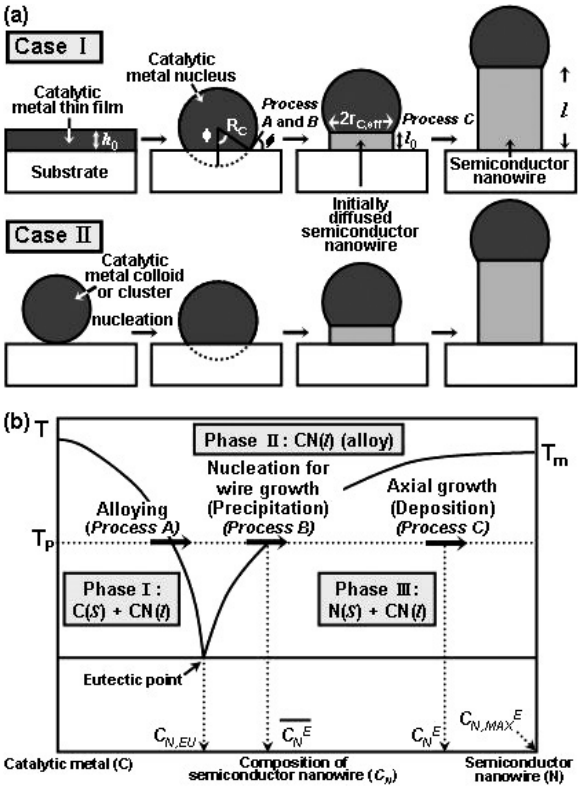

Figure 1. (a) Schematic illustrations of the VLS mechanism for the growth of the SNWs with case I: the catalytic metal thin film, and with case II: the catalytic metal colloids or clusters. (b) A typical catalytic metal–SNW binary phase diagram showing the growth procedure of the SNWs.

catalytic growth of various 1D semiconductor nanostructures has been successfully explained, although some exception to this rule was reported [18]. In the VLS mechanism, phase evolution occurs when the process temperature is elevated well above the eutectic temperature of the semiconductor–catalytic metal binary phase. The phase evolution associated with the binary phase diagram proposes that the growth of semiconductor nanowires (SNWs) hinges on a consecutive procedure, which involves the nucleation of the catalytic metal followed by alloying, the nucleation for the growth of the wires (precipitation), and the growth of the wires themselves (deposition) [2]. The schematic growth procedure of the SNWs and the binary phase diagram for a typical VLS process are illustrated in figure 1. Although numerous studies have shown that the growth of the SNWs can be explained by the VLS mechanism, few studies have attempted to explain why these SNWs have particular morphology, such as their radius, length, aspect ratio, and number density, over the surface of the substrate [19, 20]. In order to utilize the VLS mechanism to explain the growth of SNWs having a well-defined feature size in a rationally reproducible synthetic manner, more profound study is required to address the critical size of the SNWs.

In the present study, we theoretically analysed the feature size of the 1D SNWs. In particular, based on the classical thermodynamics and kinetics, we expanded the analysis of the critical radius of the SNWs, when they are grown by the catalytic metal-assisted VLS mechanism. The catalytic metal nuclei considered in this study were assumed to form prior

to the growth and nucleation of the SNWs. For the sake of simplicity, the catalytic metal was classified into two types: thin film and colloids (or cluster). The critical size of the metal nucleus is determined by several mechanisms, such as thermodynamic relationship, structural instability of metal thin film, and the radius of the starting metal nuclei in the case of metal colloids or clusters. The critical radius of the SNW is determined to have the minimum total free energy involving effects given by the initial diffusion length of the gaseous semiconductor precursor in the early growth stages. The theoretical results of the critical radius of SNWs were in good agreement with the experimental data in the literature. We also explained why the radius of the SNWs scales linearly with the radius of the metal nuclei based on experimental data in the literature. We expect the presented study to give a substantial benefit to elucidate the morphology of the SNWs involving feature sizes.

2. Determination of the critical radius of the SNWs

2.1. Case of the SNWs with the catalytic metal thin film (case I)

2.1.1. Case where the critical radius of the metal nucleus is determined prior to the number density. In the early stages of the VLS process, we considered that the catalytic metal has two types of morphology. For the first type, we considered a metal thin film that was deposited on the substrate prior to the growth of the SNWs (refer to case I in figure 1(a)). If the nucleation of the metal film (*Process B* shown in figure 1(b)) and the alloying process take place simultaneously, it cannot be confirmed that the metal nucleus has an anisotropic morphology, in the case of precipitation followed by the growth of the SNWs. Therefore, 1D uniaxial growth cannot be expected. Experimentally, it has been reported that the interface between the metal nucleus and the SNW is nearly flat [2–4]. This flat interface does not result from the simultaneous metal nucleation and alloying. Therefore, it is reasonable to suppose that the metal film is nucleated before the alloying process (*Process A* shown in figure 1(b)) [1–4].

The observed radius of the SNWs, r_{N}, where subscript N is for the nanowires, is known to be determined by the radius of the catalytic metal nucleus, R_{C} [1–4]. Additionally, the number density of the SNWs per unit surface area of the substrate with the average inter-distance between two neighbouring SNWs, D, is also determined by the number density of the metal nuclei. In order to understand the underlying factors determining such length scales, namely R_{C} and D, it is necessary to investigate the critical radius of the catalytic metal nuclei, R_{C}^{*}. In addition to its effect on D, R_{C}^{*} also determines the average volume of the metal nuclei under certain reaction conditions. Assuming that the metal thin film is mostly transformed into nuclei, R_{C}^{*} can be expressed such that $R_{\mathrm{C}}^{*} = [\frac{3\sqrt{3}D^2h_0}{4\pi(2-\cos\phi)(1+\cos\phi)^2}]^{1/3}$, where ϕ is the supplementary contact angle of the metal nucleus on the substrate and h_0 is the initial thickness of the metal film (refer to figure 1(a)). Considering this geometric relationship of $R_{\mathrm{C}}^{*} \propto D^{2/3}$, the problem whether the determination of R_{C}^{*} precedes or succeeds that of D should be addressed.

The first hypothesis corresponds to the determination of R_{C}^{*} before that of D, postulating that the critical time for the determination of R_{C}^{*} is much smaller than that of the film rupture accompanying a morphological transformation. Based on the theory of heterogeneous nucleation, R_{C}^{*} is determined to have the minimum free energy, ΔF_{C}, which can be written as follows [21]:

$$\Delta F_{\mathrm{C}} = \frac{\pi R_{\mathrm{C}}^3}{3}(2+3\cos\phi-\cos^3\phi)\Delta G_{\mathrm{VC}} + \pi R_{\mathrm{C}}^2(\gamma_{\mathrm{CS}}-\gamma_{\mathrm{SV}})\sin^2\phi + 2\pi R_{\mathrm{C}}^2\gamma_{\mathrm{CV}}(1+\cos\phi), \qquad \Delta G_{\mathrm{VC}} = -\frac{kT_{\mathrm{P}}}{\Omega_{\mathrm{C}}}\ln\left(\frac{P_{\mathrm{C}}}{P_{\mathrm{C}}^{\mathrm{E}}}\right), \tag{1}$$

where k is the Boltzman constant, T_P is the process temperature (refer to figure 1(b)), and γ is the interfacial energy, with the subscripts C, S and V corresponding to the catalytic metal nucleus, substrate, and atmosphere, respectively. The interfacial energies satisfy the relationship $\gamma_{CS} - \gamma_{SV} = \gamma_{CV} \cos\phi$. ΔG_{VC} is the chemical free energy change of the phase transformation of the metal nucleus per unit volume of the metal, Ω_C, and P_C and P_C^E are the supersaturated partial pressure and the equilibrium vapour pressure of the metal at T_P, respectively. Although the value of ϕ can vary with R_C, leading to change of shape of the metal nucleus, we assumed that the ratio between a dipolar domain interaction energy due to surface stress difference at the edge of the metal nucleus (γ_d) and γ_{CV} has a relatively small value. A value of γ_d/γ_{CV} that is sufficiently smaller than 1 gives rise to nearly constant isotropic shape (constant ϕ) of the metal nucleus on the substrate [14]. When the value of γ_d/γ_{CV} is much larger than 1, further study involving self-assembly or organization of the metal nuclei during the VLS process is required [14, 15]. Differentiating ΔF_C with respect to R_C gives R_C^* [21]:

$$R_C^* = -\frac{2\gamma_{CV}}{\Delta G_{VC}}, \tag{2}$$

where one should note that R_C^* is not necessarily equal to the minimum value of R_C, namely $R_{C,min}$ [19], under which the metal nucleus is unstable to allow the wire growth [19, 22]. In the case where $R_C = R_{C,min}$, P_C/P_C^E should be equal to P_N/P_N^E, since $R_{C,min}$ indicates that the nuclei are supersaturated with the gaseous semiconductor precursor and P_C/P_C^E for $R_C = R_{C,min}$ should be smaller than that for $R_C = R_C^*$. D is obtained from R_C^*, subsequently.

Right after the alloying process, the precipitation of the diffused out gaseous semiconductor precursor from the nucleus leads to the growth of the SNWs (*Processes B and C* shown in figure 1). Wetting of the semiconductor precursor on the bottom of the flat interface (between the catalytic metal–SNW liquid alloy (CN(l)) and the SNW solid (N(s)), where (l) and (s) denote the liquid and solid phase, respectively (refer to phases II and III in figure 1(b))) is primarily more energetically favoured than the wetting on the surface of the nucleus. Therefore the 1D anisotropy accompanying the uniaxial growth of the SNWs is attributed to the precipitation of the diffused gaseous semiconductor precursor only on the flat interface. Due to the fact that the mean free path of the diffused gaseous semiconductor precursor is sufficiently small, the initial diffusion length of the SNWs in the early stages of the growth, l_0, is limited to a certain maximum value. This value depends on the difference between the surface temperatures of the substrate and the alloy, and on the diffusivity of the gaseous semiconductor precursor, D_P. Based on the kinetic theory of an ideal gas, l_0 can be determined from D_P and the mean free time, τ_P, satisfying the relationship $l_0 = (D_P\tau_P)^{1/2}$ [23]. Using the fact that $\tau_P \sim 8 \times 10^{-10}$ s and $D_P \sim 4 \times 10^{-9}$ m^2 s^{-1} for[2] the growth of Si NWs via the catalytic VLS mechanism [1–4, 24], the value of l_0 was 1.8 nm at $T_P = 700$ K. This value of l_0 is significantly smaller than the typical radii of the metal nuclei and the SNWs.

The critical radius of the SNWs, r_C^*, can also be determined in a similar way to that used to obtain R_C^*. The free energy for the formation of the SNW of length of l_0 and radius of r_C,

[2] In calculating the value of τ_P, we examined the experimental case of SNW synthesis using incident transport inert gas (Ar) of 100 sccm at 700 K [3, 4] in a cylindrical quartz tube of 2×10^{-2} m diameter in which the pressure is maintained to have 200 Torr [3]. In this condition, the average velocity of the gaseous semiconductor precursor is estimated to be about 785 m s^{-1}, which is the sum of the average velocity of the air at 700 K (470 m s^{-1}) and the velocity given by the incident gas flux (315 m s^{-1}). In order to calculate the value of D_P, we examined the experimental case of Si NWs with the Au-assisted VLS process [3, 4]. In this case, temperature-dependent D_P was extrapolated such that $D_P = D_{P0}\exp(-E_A/kT_P)$, where D_{P0} is the diffusivity at the reference temperature and E_A is the effective activation energy for the diffusion. For simplicity, we assumed that the surface temperature of the substrate is nearly equal to that of the process temperature, T_P. Using the fact that $E_A = 1.1$ eV and $D_P = 1.1 \times 10^{-7}$ m^2 s^{-1} at $T_P = 1300$ K for the diffusion of Si in the Au matrix [24], the value of D_P could be estimated.

ΔF_{N}, can be expressed as follows:

$$\Delta F_{\mathrm{N}} = \pi r_{\mathrm{C}}^2 l_0 \Delta G_{\mathrm{VN}} + \pi r_{\mathrm{C}}^2(\gamma_{\mathrm{NS}} - \gamma_{\mathrm{SV}}) + \pi r_{\mathrm{C}}^2(\gamma_{\mathrm{NC}} - \gamma_{\mathrm{NV}}) + 2\pi r_{\mathrm{C}} l_0 \gamma_{\mathrm{NV}} + \pi(R_{\mathrm{C}}^{*2}\sin^2\phi - r_{\mathrm{C}}^2)\gamma_{\mathrm{CV}}, \qquad \Delta G_{\mathrm{VN}} = -\frac{kT}{\Omega_{\mathrm{N}}}\ln\left(\frac{P_{\mathrm{N}}}{\overline{P_{\mathrm{N}}^{\mathrm{E}}}}\right), \tag{3}$$

where P_{N} is the supersaturated partial pressure and $\overline{P_{\mathrm{N}}^{\mathrm{E}}}$ is the equilibrium vapour pressure of the gaseous semiconductor precursor, when the composition of the SNW, C_{N}, is equal to that on the boundary between phases II and III at $T = T_{\mathrm{P}}$, $\overline{C_{\mathrm{N}}^{\mathrm{E}}}$ (refer to figure 1(b)), and ΔG_{VN} is the free energy required for the phase transformation of the SNW per unit volume of the SNW, Ω_{N}. Given the contact angle of the liquid SNW precursor droplet on the substrate at T, θ_{N}, the interfacial energies satisfy the relationship $\gamma_{\mathrm{NS}} = \gamma_{\mathrm{SV}} - \gamma_{\mathrm{NV}}\cos\theta_{\mathrm{N}}$. Differentiating ΔF_{N} with respect to r_{C} gives r_{C}^* as follows:

$$r_{\mathrm{C}}^* = \frac{\gamma_{\mathrm{NV}}}{\gamma_{\mathrm{NV}}\left(\frac{2+\cos\theta_{\mathrm{N}}}{l_0}\right) - \Delta G_{\mathrm{VN}}} = \frac{\Omega_{\mathrm{N}}\gamma_{\mathrm{NV}}}{\Omega_{\mathrm{N}}\gamma_{\mathrm{NV}}\left(\frac{2+\cos\theta_{\mathrm{N}}}{l_0}\right) + kT\left[\ln\left(\frac{P_{\mathrm{N}}^{\mathrm{E}}}{\overline{P_{\mathrm{N}}^{\mathrm{E}}}}\right) + \ln\left(\frac{P_{\mathrm{N}}}{P_{\mathrm{N}}^{\mathrm{E}}}\right)\right]}, \tag{4}$$

where $P_{\mathrm{N}}^{\mathrm{E}}$ is the nonequilibrium vapour pressure of the gaseous semiconductor precursor at $C_{\mathrm{N}} = C_{\mathrm{N}}^{\mathrm{E}}$ (refer to figure 1(b)). One should note that r_{C}^* does not indicate the thermodynamically allowed minimum value of r_{C}, namely $r_{\mathrm{C,min}}$, as is the case where R_{C}^* and $R_{\mathrm{C,min}}$ are compared, since $r_{\mathrm{C,min}} = \frac{\Omega_{\mathrm{N}}\gamma_{\mathrm{NV}}}{kT\left[\ln\left(\frac{P_{\mathrm{N}}^{\mathrm{E}}}{\overline{P_{\mathrm{N}}^{\mathrm{E}}}}\right)+\ln\left(\frac{P_{\mathrm{N}}}{P_{\mathrm{N}}^{\mathrm{E}}}\right)\right]}$ [19, 22] is greater than r_{C}^*.

In figure 2, r_{C}^* was plotted as a function of T_{P} in the case of Si NWs. For the sake of simplicity, equation (4) was rewritten as $r_{\mathrm{C}}^* = \frac{\Omega_{\mathrm{N}}\gamma_{\mathrm{NV}}}{\Omega_{\mathrm{N}}\gamma_{\mathrm{NV}}\left(\frac{2+\cos\theta_{\mathrm{N}}}{l_0}\right)+kT\ln\left(\frac{P_{\mathrm{N}}^{\mathrm{E}}}{\overline{P_{\mathrm{N}}^{\mathrm{E}}}}\right)}$ assuming that the effect of a liquid droplet of the SNW of finite size is negligible [19]. The term $\ln(P_{\mathrm{N}}^{\mathrm{E}}/\overline{P_{\mathrm{N}}^{\mathrm{E}}})$ in equation (4) can be expressed as $\ln\{[\zeta_{\mathrm{N}}(C_{\mathrm{N,max}}^{\mathrm{E}})C_{\mathrm{N,max}}^{\mathrm{E}}]/[\zeta_{\mathrm{N}}(\overline{C_{\mathrm{N}}^{\mathrm{E}}})\overline{C_{\mathrm{N}}^{\mathrm{E}}}]\}$ [19], where $\zeta_{\mathrm{N}}(C_{\mathrm{N,max}}^{\mathrm{E}})$ and $\zeta_{\mathrm{N}}(\overline{C_{\mathrm{N}}^{\mathrm{E}}})$ are the extended chemical activity coefficients of the SNW at $C_{\mathrm{N}} = C_{\mathrm{N,max}}^{\mathrm{E}}$ and $C_{\mathrm{N}} = \overline{C_{\mathrm{N}}^{\mathrm{E}}}$, respectively (refer to figure 1(b)). In a typical binary phase diagram, $\zeta_{\mathrm{N}}(C_{\mathrm{N,max}}^{\mathrm{E}})/\zeta_{\mathrm{N}}(\overline{C_{\mathrm{N}}^{\mathrm{E}}})$ is nearly 1, and $C_{\mathrm{N,max}}^{\mathrm{E}}$ can be approximated to 1 (refer to figure 1(b)) [19], and $\overline{C_{\mathrm{N}}^{\mathrm{E}}}$ exhibits an exponential behaviour with respect to T_{P} such that $\log_{10}\overline{C_{\mathrm{N}}^{\mathrm{E}}} = -(A/T_{\mathrm{P}}) + B$ [24], when C_{N} is greater than the composition of the eutectic point, $C_{\mathrm{N,eu}}$. Given the fact that $\overline{C_{\mathrm{N}}^{\mathrm{E}}} \sim 0.64$ at $T_{\mathrm{P}} = 700$ K (calculated by us) [19, 25] and $\overline{C_{\mathrm{N}}^{\mathrm{E}}} \sim C_{\mathrm{N,max}}^{\mathrm{E}} \sim 1$ at $T_{\mathrm{P}} = 1683$ K (this temperature is equal to the melting point of Si, T_{m}), the values of A and B were calculated as $A = 237.69$ K and $B = 0.14$, respectively.

In order to verify our theoretical prediction of r_{C}^*, we compared the prediction with experimental data of different synthetic cases of the metal-catalysed VLS growth of Si NWs obtained from the literature. Figure 2(a) shows the dependence of r_{C}^* on T_{P} for Si NWs grown by an Au-catalysed VLS process with experimental data for the minimum value of the radius of the Si NWs [4–6]. It should be noted that the effective critical radius of Si NWs, $r_{\mathrm{C,eff}}^*$, for the experimental data is smaller than the observed minimum values of r_{C}^*. This difference is mainly due to an outer layer (amorphous sheath or oxide layer) surrounding the crystalline Si core. The existence of this layer can be confirmed by the high-resolution transmission electron microscope (HRTEM) images of the wires reported in the literature [4–6]. The thickness of the outer layer did not vary case by case, since it is determined by the surface properties and reaction kinetics. Since $r_{\mathrm{C,eff}}^*$ is smaller than the observed minimum value of r_{C}^*, theoretical prediction considering l_0 is matched better with the experimental data than the prediction

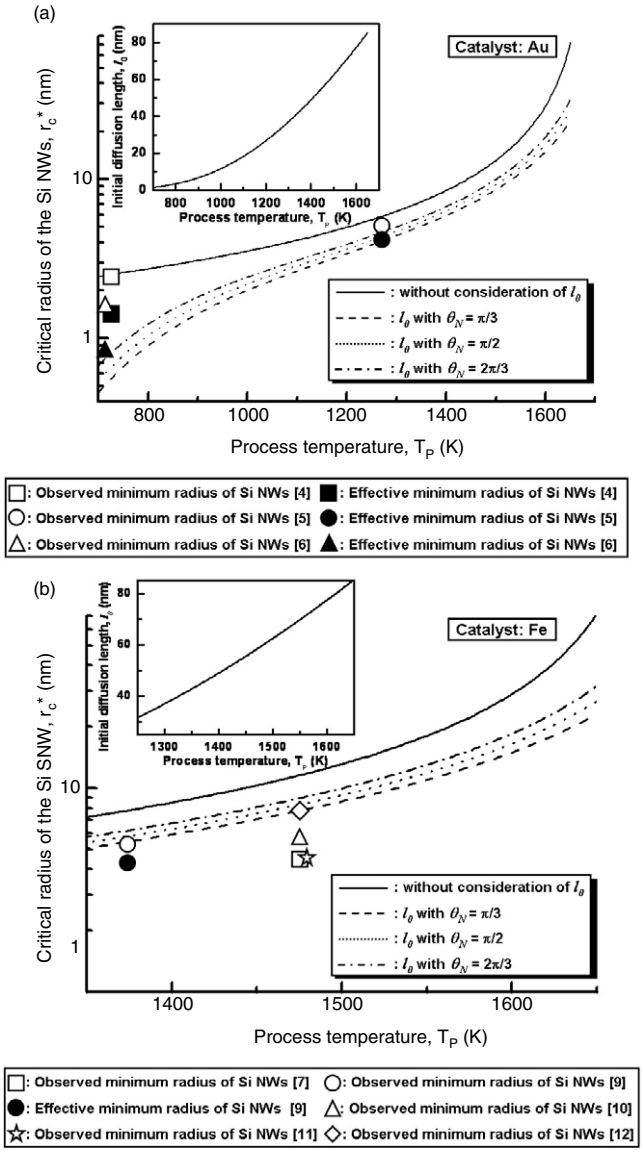

Figure 2. Theoretical prediction of the critical radius of the SNW, r_C^*, in the case of Si NWs grown by the Au (a) and Fe-assisted (b) VLS mechanism with different values of the contact angle of the SNW on the substrate, θ_N. In order to calculate r_C^*, the surface energy of the SNW, γ_{NV}, was assumed to be 1.61 N m^{-1} [19], with the atomic volume of Si, Ω_N of 6.71 $\times$ 10^{-30} m^3 [24], and the maintained process pressure in the reactor of 200 Torr [3]. Dark symbols are for the effective minimum radius for the crystalline Si core, while open symbols are for the observed minimum value of the radius of Si NWs including the outer layer obtained from the literature [8–10].

without consideration of l_0. Shown in figure 2(b) is the dependence of r_C^* on T_P for the Si NWs grown by an Fe-catalysed VLS process, and the theoretical prediction considering l_0 shows the more satisfactory agreement with the experimental data than the conventional theory without consideration of l_0, although some experimental data are somewhat smaller than the

predicted values. For some cases, experimental data of r_C^* were considered to be $r_{C,eff}^*$ based on the HRTEM analysis presented in the literature [7, 10–12]. A notable finding in figure 2 is that an increase in the value of θ_N leads to an increase in the value of r_C^*. This means that the higher the surface energy barrier for the anisotropic growth of the wire on the substrate, the larger the radius of the wire. In the plots shown in figure 2, it is noteworthy that the initial diffusion of the gaseous semiconductor precursor results in a reduction in the value of r_C^*, even though r_C^* is smaller than $r_{C,min}$, which corresponds to the stable growth of the SNWs. This is mainly due to the drastic increase in l_0 which occurs as T_P increases, as shown in the inset in figure 2.

As many experimental studies have reported [1–4], r_C^* is smaller than R_C^* and, therefore, the effective radius of the SNW, $r_{C,eff}$, is not theoretically confirmed to be equal to $R_C^* \sin\phi$. Based on equation (4), r_C^* is equal to $r_{C,eff}$ and independent of R_C^*. This indicates that mushroom-like SNWs with a truncated sphere-shaped metal cap can form. However, this shape of SNWs has not been observed. Exceptionally, in the case where $r_C^* > R_C^* \sin\phi$, the gaseous semiconductor precursor which diffuses out of CN(l) may be coerced to mirror the metal nucleus, due to the fact that there will be less free energy involved in the N(s)–CN(l) interface. Then, $r_{C,eff}$ is equal to $R_C^* \sin\phi$.

2.1.2. Case where the determination of the number density precedes that of the critical radius of the metal nucleus. In the reverse case of the first hypothesis, we consider that the critical length resulting from the structural instability in the metal thin film determines the value of R_C^*. Metal film thinner than 100 nm suffers from structural instability, when they are in the fluidic state heated well above certain critical temperature [26, 27]. According to the spinodal dewetting theory [28], the morphological evolution of the metal film from the state of fast surface undulation to that of nucleation can be elucidated based on the governing length scale, λ_C, which mainly determines D such that $\lambda_C \sim D$. Sufficiently thin metal film satisfies the following relationship: $\lambda_C = \frac{4\pi^{3/2}\gamma_{CV}^{1/2}}{A_{eff}^{1/2}} h_0^2$ [27], where A_{eff} is the effective non-retarded Hamaker constant of the metal film with the surrounding matter for van der Waals interaction. For a typical catalytic metal film whose thickness ranges from 1 to 10 nm, the Lennard-Jones-type repulsion force, $-C_L/h_0^9$, where C_L is a constant with a value of approximately 10^{-76} J m^6 [23], can be neglected, since the van der Waals force exceeds the repulsion force by four orders of magnitude. According to the capillary theory [28, 29], the exponentially evolving amplitude of the surface wave resulting from the instability causes λ_C to emerge in the critical time, $\tau_C = 3h_0^5\pi^2\gamma_{CV}^2/\upsilon A_{eff}^2$. υ is the propagation velocity of the surface wave that is determined by the ratio of γ_{CV} to the viscosity of the fluidic metal thin film, η. Given the values $\eta = 5.38 \times 10^{-3}$ N s m^{-2} [30], $\gamma_{CV} = 1.15$ N m^{-1} [31], and $A_{eff} = 4.10 \times 10^{-19}$ J [32] of Au, τ_C is calculated to attain 278 ns when $h_0 = 3$ nm. For the value of $\gamma_{CV} = 1.15$ N m^{-1}, we neglected the reduction of γ_{CV} due to the alloying [31]. This value of τ_C is sufficiently small for the rupture of the metal film to occur prior to the alloying process. If the number density of the holes in the metal film caused by the defects on the substrate is sufficiently small to neglect its effect in the formation of the metal nucleus, R_C^* can be written using the geometric relationship as follows:

$$R_C^* = \left[\frac{12\sqrt{3}\pi^2\gamma_{CV}}{A_{eff}(2-\cos\phi)(1+\cos\phi)^2} h_0^5\right]^{1/3}. \tag{5}$$

R_C^* obtained from equation (5) might be smaller than R_C^* from equation (2), which corresponds to thermodynamically unstable metal nuclei. However, in the case where the determination of D precedes that of R_C^*, R_C^* is determined by the kinetic effect caused by the structural instability prior to thermodynamic effect. In figure 3, R_C^* calculated from equation (5) was plotted as a

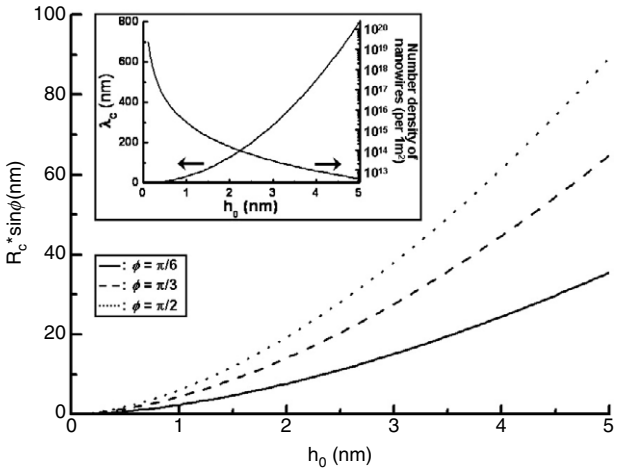

Figure 3. Behaviour of the effective radius of the SNW, $r_{C,eff}$, when $r_C^* > R_C^*$ ($r_{C,eff} = R_C^* \sin\phi$), which is determined by the radius of the metal nucleus, R_C^*, and the complementary contact angle of the metal nucleus on the substrate, ϕ, as a function of the initial thickness of the catalytic metal thin films (h_0) with different values of ϕ for the case where the determination of the inter-distance between two neighbouring metal nucleus, D, precedes that of R_C^*, in case I. The inset shows behaviours of D calculated by the critical length scale given by the structural instability in the metal thin film, $\lambda_C = D$ (left), and the number density of the nuclei (right) as a function of h_0.

function of h_0 in the case of Au with different values of ϕ. For a thin metal film satisfying a relationship of $R_C^* < r_C^*$, the precipitation of the diffused gaseous semiconductor precursor occurs only on the CN(l)–N(s) interface, with the result that $r_{C,eff} = R_C^* \sin\phi$, subsequent to the precipitation. In this regime, the shape of the SNW reflects that of the metal nucleus. On the other hand, in the case of a thick film for which $R_C^* > r_C^*$, mushroom-like SNWs with a truncated sphere-shaped metal cap would form, as analysed in the first hypothesis.

2.2. Case of the SNW with the catalytic metal colloids or cluster (case II)

The catalytic metal nuclei can be prepared by the dispersion of the colloidal metal particles or cluster over the substrate [1–4]. In this case, the number density and the radius of the metal nucleus are intensively determined in a controllable manner. And the number density of the SNWs is nearly equal to that of the metal colloids or clusters [1–4]. Considering the radius of the SNW, a method of obtaining r_C^* similar to that described in the above section 2.1 can be applied. The literature reporting the growth of the SNWs using catalytic metal colloids or clusters shows that the SNW mirrors the metal colloids or clusters. This indicates that $R_C^* < r_C^*$ satisfying $r_{C,eff} = R_C^* \sin\phi$. This mirroring behaviour, despite the fact that R_C^* seemed to be smaller than r_N, can be explained by the fact that the SNW is comprised of a crystalline core and an amorphous sheath with a thickness of r_a, based on the examination of the high-resolution transmission electron microscope (HRTEM) images of the structures [1–4]. The formation of the amorphous sheath has been mainly ascribed to the alloying or post-growth oxidation of the metal catalytic nucleus–semiconductor precursor [1–4]. Therefore, $r_{C,eff}$ is smaller than r_N (refer to the right inset of figure 4). And it is reasonable to consider that r_a is independent of r_C^* and R_C^*, since r_a is determined by the surface properties of the structures and synthetic conditions such as T_P, the partial vapour pressure of the reactant, the flow rate of the gaseous reactant, etc. Therefore, r_N should be expressed as $r_N = r_{C,eff} + r_a = R_C^* \sin\phi + r_a$.

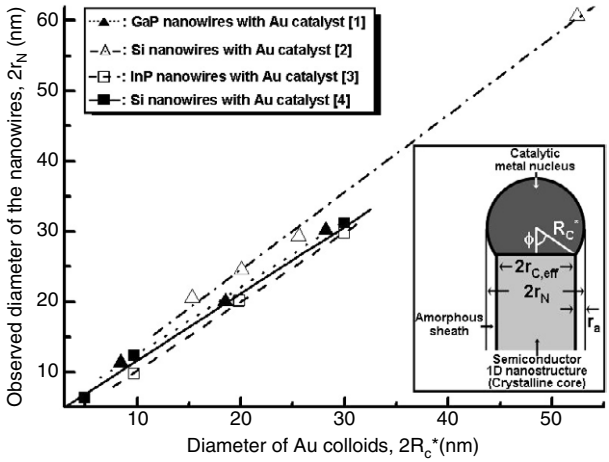

Figure 4. Linear correlation between the critical diameter of the metal nucleus, $2R_C^*$, and the observed diameter of the SNW, $2r_N$ satisfying $2r_N = 2R_C^* \sin\phi + 2r_a$, for four kinds of SNW grown by the Au colloids (or cluster)-assisted VLS mechanism. Experimental data described by symbols are obtained from the literature (observed values of r_a were obtained from the HRTEM images shown in the literature) [1–4]. The lower right inset is a schematic illustration of the SNW comprised of a crystalline core coated by an amorphous sheath with a constant thickness, r_a.

The comparisons in figure 4 between this relationship and different experimental data obtained from the literature show linearly scaling behaviours of r_N with R_C^*. In the linearly fitted plots, the values of ϕ and $2r_a$ can be calculated. As shown in table 1, assuming that r_a is a constant, we found that this relationship can explain why r_N is somewhat larger than R_C^* for various SNWs grown by the Au colloids (cluster)-assisted VLS mechanism. We also found that the catalytic metal nucleus has a truncated sphere shape accompanied by a particular value of ϕ, as we had assumed. Although some calculated values of r_a are smaller and some calculated values of ϕ are greater or smaller than the observed values of r_a and ϕ (measured by us) (table 1), the well-matched linear relationship between R_C^* and r_N, accompanying good congruities of the calculated values of r_a and ϕ with the observed values of r_a and ϕ, respectively, indicates that $r_{C,eff} = R_C^* \sin\phi$.

Additionally, for the catalytic metal nucleus, we can think of the interface between CN(l) and N(s) as being flat rather than curved. If the interface is curved, the radius of the SNW is limited, such that $r_C^* \leqslant [2R_C^* l_0 - l_0^2]^{1/2}$, since l_0 is much smaller than R_C^*, and the SNWs do not mirror the metal colloids. The flat interface of the alloy might be attributed to the partial melting (or nucleation) of the metal nucleus on the substrate (refer to case II in figure 1(a)). This is also supported by the calculation results shown in table 1, in which the values of ϕ combined with those of R_C^* determine the interface area. Interestingly, the calculated and observed values of ϕ in table 1 are somewhat different, in spite of the fact that the experimental data used in table 1 commonly adopted Au as a catalyst. This difference in the values of ϕ can be explained by the differences in the synthetic conditions.

3. Summary

We studied the critical radius of semiconductor nanowires (SNWs), r_C^*, grown by the metal-catalyst assisted vapour–liquid–solid (VLS) mechanism. The thermodynamic analysis showed that r_C^* is determined by the surface and interfacial free energies of the metal nucleus, substrate and the SNWs, along with the phase transformation free energy, assuming the initial diffusion

Table 1. Calculation results of the complementary contact angle of the catalytic metal (Au) on the substrate for four kinds of experimental study [1–4], ϕ, that is responsible for the determination of the effective radius of the SNW, $r_{C,eff} = R_C^* \sin\phi$, when $r_C^* > R_C^*$, where R_C^* is the critical radius of the metal nucleus. Calculated values of the thickness of the amorphous sheath, r_a, around the crystalline core of the SNW are obtained from figure 4. Observed values (experimental data given by the examination the HRTEM images obtained from the literature) of ϕ and r_a are also shown for the comparison with the calculated values of ϕ and r_a. The calculated values of ϕ and r_a in the case of Si NWs reported in [2] are based on the relationship of the linear extrapolation of the experimental data stated by authors.

System	Calculated value of ϕ (deg)	Observed value of ϕ (deg)	Calculated value of r_a (nm)	Observed value of r_a (nm)	Reference number
GaP nanowires with Au colloids	71.59	68.0	1.55 ± 0.58	4.45 ± 1.12	[1]
Si nanowires with Au clusters	90 [2]	86.5	2.50 ± 0.75 [2]	2.01 ± 0.55	[2]
InP nanowires with Au colloids	78.63	63.5	0.49 ± 0.21	2.23 ± 0.55	[3]
Si nanowires with Au colloids	72.43	74.0	1.05 ± 0.50	1.38 ± 0.56	[4]

length of the supersaturated gaseous semiconductor precursor. In the case of a catalytic metal thin film for which the determination of R_C^* precedes that of the number density, we found that R_C^* is thermodynamically determined. There is not necessarily any correlation between r_C^* and R_C^*, if $r_C^* < R_C^*$, leading to $r_{C,eff} = r_C^*$, where $r_{C,eff}$ is the effective radius of the SNW. In contrast, $r_{C,eff}$ is proportional to R_C^*, when $r_C^* > R_C^*$. In the case where the number density is structurally determined prior to R_C^*, R_C^* was calculated from the characteristic wavelength given by the structural instability in the thin film. In the case where catalytic metal colloids or clusters are involved, we found that R_C^* and the observed radius of the SNW, r_N, are linearly correlated, assuming the existence of an amorphous sheath around the crystalline core. It was shown that the suggested model was matched well with the experimental data in the literature. It was also found that the SNWs mirror the metal colloids or clusters, assuming that the amorphous sheath has a constant thickness. The theoretical analysis on the critical radius of the SNWs presented here would give a substantial benefit to those who want to control the uniformity of the feature size in a predictable experimental manner and to utilize well-defined 1D semiconductor nanostructures involving nanowires grown by the catalytic VLS mechanism.

References

[1] Gudiksen M S and Lieber C M 2000 *J. Am. Chem. Soc.* **122** 8801
[2] Wu Y and Yang P 2001 *J. Am. Chem. Soc.* **123** 3165
[3] Gudiksen M S, Wang J and Lieber C M 2001 *J. Phys. Chem.* B **105** 4062
[4] Cui Y, Lauhon L J, Gudiksen M S, Wang J and Lieber C M 2001 *Appl. Phys. Lett.* **78** 2214
[5] Xing Y J, Yu D P, Xi Z H and Xue Z Q 2003 *Appl. Phys.* A **76** 551
[6] Wu Y, Cui Y, Hyunh L, Barrelet C J, Bell D C and Lieber C M 2004 *Nano Lett.* **4** 433
[7] Morales A M and Lieber C M 1998 *Science* **279** 208
[8] Duan X, Huang Y, Cui Y, Wang J and Lieber C M 2001 *Nature* **409** 66
[9] Gu Q, Dang H, Cao J, Zhao J and Fan S 2000 *Appl. Phys. Lett.* **76** 3020
[10] Feng S Q, Yu D P, Zhang H Z, Bai Z G and Ding Y J 2000 *J. Cryst. Growth* **209** 513
[11] Huang Y, Duan X, Cui Y, Lauhon L, Kim K and Lieber C M 2001 *Science* **294** 1313
[12] Yang W H, Wu S J, Chiu H S, Lin P I and Chen Y T 2004 *J. Phys. Chem.* B **108** 846
[13] Wang N, Tang Y H, Zhang Y F, Lee C S and Lee S T 1998 *Phys. Rev.* B **58** R16024
[14] Liu F 2002 *Phys. Rev. Lett.* **89** 246105

[15] Bai L, Tersoff J and Liu F 2004 *Phys. Rev. Lett.* **92** 225503
[16] Tersoff J and Tromp R M 1993 *Phys. Rev. Lett.* **70** 2782
[17] Wagner R S and Ellis W C 1964 *Appl. Phys. Lett.* **4** 89
[18] Dick K A, Deppart K, Martensson T, Mandl B, Samuelson L and Seifert W 2005 *Nano Lett.* **5** 761
[19] Tan T Y, Li N and Gösele U 2003 *Appl. Phys. Lett.* **83** 1199
[20] Kwon S J and Park J G 2005 *J. Chem. Phys.* **122** 214714
[21] Ohring M 2002 *Materials Science of Thin Films: Deposition and Structure* (San Diego, CA: Academic)
[22] Givargizov E I 1975 *J. Cryst. Growth* **31** 20
[23] Ferry D K and Goodnick S M 1997 *Transport in Nanostructures* (Cambridge: Cambridge University Press)
[24] Shackelford J F and Alexander W 2001 *Materials Science and Engineering Handbook* 3rd edn (New York: CRC Press)
[25] Massalski T B, Okamoto H, Subramian P R and Kacprzak L 1990 *Binary Phase Diagrams* 2nd edn (Metals Park, OH: ASM International)
[26] Srolovitz D J and Goldiner M G 1995 *J. Met.* **3** 31
[27] Bischof J, Scherer D, Herminghaus S and Leiderer P 1996 *Phys. Rev. Lett.* **77** 1536
[28] Xie R, Karim A, Douglas J F, Han C C and Weiss R A 1998 *Phys. Rev. Lett.* **81** 1251
[29] Suh K Y and Lee H H 2002 *J. Chem. Phys.* **117** 6266
[30] Iida T and Guthrie R I L 1987 *The Physical Properties of Liquid Metals* (Oxford: Oxford University Press)
[31] Egry I, Lohoefer G and Jacobs G 1995 *Phys. Rev. Lett.* **75** 4043
[32] Israellachivili J N 1992 *Intermolecular and Surface Forces* 2nd edn (New York: Academic)